Journal of Magnetic Resonance 214 (2012) 151–158

Contents lists available at SciVerse ScienceDirect

Journal of Magnetic Resonance

journal homepage: www.elsevier.com/locate/jmr

Practical choice of ^{1}H–^{1}H decoupling schemes in through-bond ^{1}H–{X} HMQC experiments at ultra-fast MAS

Yusuke Nishiyama [a,*], Xingyu Lu [b], Julien Trébosc [b], Olivier Lafon [b], Zhehong Gan [c], P.K. Madhu [d], Jean-Paul Amoureux [b]

[a] JEOL RESONANCE Inc., 3-1-2 Musashino, Akishima, Tokyo 196-8558, Japan
[b] UCCS (CNRS-8181), Lille North of France University, Villeneuve d'Ascq 59652, France
[c] Center of Interdisciplinary Magnetic Resonance, NHMFL, Tallahassee, FL 32310, USA
[d] Department of Chemical Sciences, TIFR, Colaba, Mumbai 400 005, India

ARTICLE INFO

Article history:
Received 9 June 2011
Revised 5 October 2011
Available online 9 November 2011

Keywords:
Solid-state NMR
^{1}H
Very fast MAS
1 mm MAS
HMQC
CRAMPS

ABSTRACT

Three ^{1}H–^{1}H homonuclear dipolar decoupling schemes for ^{1}H indirect detection measurements at very fast MAS are compared. The sequences require the following conditions: (i) being operable at very fast MAS, (ii) a long T_2' value, (iii) a large scaling factor, (iv) a small number of adjustable parameters, (v) an acquisition window, (vi) a low rf-power requirement, and (vii) a z-rotation feature. To satisfy these conditions a modified sequence named TIlted Magic-Echo Sandwich with *zero* degree sandwich pulse (TIMES$_0$) is introduced. The basic elements of TIMES$_0$ consist of one sampling window and two phase-ramped irradiations, which realize alternating positive and negative 360° rotations of ^{1}H magnetization around an effective field tilted with an angle θ from the B_0 axis. The TIMES$_0$ sequence benefits from very large chemical shift scaling factors at ultra-fast MAS that reach $\kappa_{cs} = 0.90$ for $\theta = 25°$ at $\nu_r = 80$ kHz MAS and only four adjustable parameters, resulting in easy setup. Long $\kappa_{cs}T_2'$ values, where T_2' is a irreversible proton transverse relaxation time, greatly enhance the sensitivity in ^{1}H–{^{13}C} through-bond J-HMQC (Heteronuclear Multiple-Quantum Coherence) measurements with ^{1}H–^{1}H decoupling during magnetization transfer periods. Although similar sensitivity can be obtained with through-space D-HMQC sequences, in which ^{13}C–^{1}H dipolar interactions are recoupled, J-HMQC experiments incorporating ^{1}H–^{1}H decoupling benefit from lower t_1-noise, more uniform excitation of both CH, CH$_2$ and CH$_3$ moieties, and easier identification of through-bond connectivities.

1. Introduction

Sensitivity enhancement by indirect detection of ^{13}C and ^{15}N spectra via ^{1}H nuclei is a well established method in solution nuclear magnetic resonance (NMR) experiments [1–3]. Since the magnetization is transferred via J-coupling, the resulting 2D spectra show through-bond correlations which are useful for resonance assignments. The sensitivity enhancements are due to high natural abundance (≈99.99%) and gyromagnetic ratio of ^{1}H. The narrow line-widths of ^{1}H nuclei and their long T_2' values, which are much longer than the magnetization transfer periods, even for small J couplings, greatly contribute to sensitivity enhancement. However, high natural abundance and gyromagnetic ratio also lead to strong ^{1}H–^{1}H homonuclear dipolar interactions, which are fortunately averaged out by fast isotropic tumbling motions in the solution state. On the other hand, these interactions induce rapid spin diffusion among ^{1}H nuclei in rigid-solid samples, resulting in short T_2' relaxation times, typically less than tens of micro-seconds, and in broad ^{1}H line-widths usually more than 50 kHz under static conditions. These two facts quickly quench ^{1}H magnetization during the magnetization transfer periods and signal acquisition. Thus, indirect detection via ^{1}H nuclei in solid state seems not to be as efficient as in solution state, especially if ^{1}H–^{1}H interactions are not greatly decreased [4–11].

Decoupling of ^{1}H–^{1}H homonuclear dipolar interactions is hence essential to achieve efficient indirect-detection via ^{1}H nuclei in solids. Theoretically, ^{1}H–^{1}H homonuclear decoupling is easily realized by only applying an infinitely fast magic-angle spinning (MAS) sample rotation. Recently, rotation frequencies have largely increased with the advent of small diameter rotors [12]. However, even at $\nu_r = 80$ kHz, which is the fastest spinning frequency commercially available now [13], ^{1}H–^{1}H interactions still show significant effect on ^{1}H line-width and T_2' value (see Figs. 2 and 4). Therefore, rf irradiations, as well as MAS, are needed to decouple efficiently these interactions. Numerous ^{1}H–^{1}H decoupling schemes have been designed from the early stage of NMR [14–49]. Recently, sophisticated methods were developed by considering rf and mechanical averaging

* Corresponding author. Fax: +81 42 546 8068.
E-mail address: yunishiy@jeol.co.jp (Y. Nishiyama).

1090-7807/$ - see front matter © 2011 Elsevier Inc. All rights reserved.
doi:10.1016/j.jmr.2011.10.014

simultaneously [25–32]. Synchronized [29–32] or non-synchronized [33,34,38–41] Combined Rotation And Multiple Pulse Spectroscopy (CRAMPS) methods with ultra-fast MAS above $\nu_r = 60$ kHz have been introduced, including SAM [29–31], RN_n^{ν} [32], wPMLG$_{pp}^{x\bar{x}}$ [33], eDUMBO [38,40], and TIMES [41]. All of these rf-assisted ^{1}H–^{1}H decoupling methods suppress ^{1}H–^{1}H dipolar interactions, but inevitably introduce scaling down of ^{1}H isotropic chemical shifts, as well as of ^{13}C–^{1}H J-couplings, by a factor of κ_{cs}. As CRAMPS direct ^{1}H signal acquisition introduces a large additional noise and artifacts, very fast MAS alone is frequently preferred for line-narrowing in the direct ^{1}H dimension [5,50–52]. To our knowledge, no measurement of T_2' enhancement by ^{1}H–^{1}H dipolar decoupling during magnetization transfer periods has been reported for ^{13}C indirect detection in fast MAS through-bond ^{1}H–{^{13}C} correlation experiments. Although, this T_2' enhancement has been demonstrated in the ^{13}C direct detection scheme at moderate MAS frequencies [53].

In this article, we investigate the ^{1}H–^{1}H decoupling schemes during the magnetization transfer periods in through-bond ^{1}H–{^{13}C} correlation experiments with indirect ^{13}C observation via ^{1}H nuclei. The decoupling scheme should: (i) work well at very fast MAS to narrow the ^{1}H line-widths, (ii) enhance the T_2' relaxation time to reduce signal decay during the magnetization transfer periods, and (iii) show a large scaling factor to shorten the magnetization transfer periods. In addition to these features, it is preferable that the decoupling scheme presents several additional features: (iv) a small number of parameters to be optimized, (v) an acquisition window enabling a direct 1D observation during optimization, (vi) a moderate rf power requirement, and (vii) an effective global precession of the spins around B_0, usually called a z-rotation. Features (iv) and (v) enable a fast optimization of experimental parameters by directly observing 1D spectra. Features (vi) and (vii) are preferable to avoid sample heating and artificial modulations due to zero or symmetrical false ^{1}H peaks, respectively. Usually, feature (vii) presents the disadvantage of reducing the scaling factor; but it has experimentally been found that this is not the case for very fast MAS [49], as shown below.

First, we investigate two ^{1}H–^{1}H decoupling schemes, wPMLG$_{pp}^{x\bar{x}}$ and TIMES, at very fast MAS. We also introduce a new version of TIMES, named TIMES$_0$, in which the sandwich pulses are removed, thus leading to favorable features for ^{1}H–{^{13}C} J-HMQC (Heteronuclear Multiple-Quantum Coherence) experiments at ultra-fast MAS. To conclude, we compare two different ^{1}H–{^{13}C} indirect HMQC observations, either based on through-bond or on through-space correlations.

2. ^{1}H–^{1}H homonuclear decoupling schemes

In the article, we focus on three windowed non rotor-synchronized ^{1}H–^{1}H decoupling schemes: wPMLG$_{pp}^{x\bar{x}}$, TIMES and TIMES$_0$ (Fig. 1a). Indeed, these sequences work well at very fast MAS, enhance the T_2' relaxation time, have an acquisition window, and offer an effective z-rotation for ^{1}H magnetization [33,41]. The gray sandwich pulses are removed in wPMLG$_{pp}^{x\bar{x}}$ and TIMES$_0$, and hence, experimentally their pulse sequences are similar. However, as shown below, the two basic concepts of wPMLG$_{pp}^{x\bar{x}}$ and TIMES$_0$ sequences are very different and their optimizations do not only correspond to a re-parameterization process. In the three sequences the magnetization is rotated during each τ_p period with an angle ψ around the effective field, which is tilted from the B_0 axis by the angle θ. Every cycle period, $\tau_c = 2(\tau_p + \tau_\theta) + \tau_w$, the global rotation is cancelled in each R or $\bar{R}$ unit, since the direction of the rotation in the second τ_p period is reversed. Thus, the interaction frame of the rf-field is coincident with the rotating frame in each sampling window, τ_w, where the NMR signal is sampled. An effective z-rotation for the magnetization is achieved by applying two effective fields symmetrical with respect to B_0 during two consecutive τ_c periods [46–48]. The major difference between these methods is the ψ angle value and the presence or absence of sandwich pulses. These sequences are summarized in Table 1.

Let's first analyze the wPMLG$_{pp}^{x\bar{x}}$ sequence, which is composed with the R $\left(\text{wPMLG}_p^x\right)$ and $\bar{R}$ $\left(\text{wPMLG}_p^{\bar{x}}\right)$ units. Each unit was originally designed by adding an acquisition window to the windowless PMLG sequence, which is essentially the same as the Frequency-Switched Lee–Goldburg (FSLG) sequence [20]. In FSLG, the tilt of the effective field is achieved by an off-resonance irradiation at ν_{off} frequency, whereas PMLG employs an on-resonance irradiation and the tilt of the effective field results from a sweep of the rf phase from 0 to ϕ_{last} [22]:

$$\phi_{last}(^\circ) = 360 \cdot \nu_{off} \cdot \tau_p, \tag{1}$$

where τ_p is the length of the ramped on-resonance irradiation. The rotation angle ψ about the effective field during τ_p is described by:

$$\psi(^\circ) = 360 \cdot \nu_{eff} \cdot \tau_p = 360 \cdot \sqrt{\nu_{1p}^2 + \nu_{off}^2} \cdot \tau_p = \sqrt{(360\nu_{1p}\tau_p)^2 + \phi_{last}^2}, \tag{2}$$

where ν_{1p} is the strength of the on-resonance B_1 field during the phase ramp. ν_{eff} is the strength of the effective field, which is tilted by the angle θ with respect to the B_0 magnetic field:

$$\tan\theta = \frac{\nu_{1p}}{\nu_{off}}. \tag{3}$$

$\theta = \theta_m = 54.74^\circ$ is used in FSLG and PMLG to achieve the Lee–Goldburg condition, and the theoretical length of the phase ramp irradiation is chosen to achieve a full $\psi = 360^\circ$ rotation about the effective field, thus leading to $\tau_p = 1/\nu_{eff} = 1/\left(\nu_{off}^2 + \nu_{1p}^2\right)^{1/2}$ and $\phi_{last} = 208^\circ$. In practice, wPMLG$_{pp}^{x\bar{x}}$ is experimentally optimized by changing τ_p, while keeping the phase ramp final value of $\phi_{last} = 208^\circ$. This optimization leads to a concurrent variation of the offset frequency, ν_{off}, and of the θ and ψ angles. Indeed, after optimization, the experimentally optimized τ_p value tends to become shorter than its theoretical value [54], which corresponds to a θ angle smaller than θ_m (Eqs. (1), (3)), and to a ψ angle smaller than 360° (Eq. (2)).

With TIMES and TIMES$_0$, the effective rotation is always kept equal to $\psi = 360^\circ$ by changing not only the length of the on-resonance irradiation, but also simultaneously the phase sweep value (Eq. (2)) to:

$$\phi_{last}(^\circ) = 360.\left(1 - \tau_p^2\nu_{1p}^2\right)^{1/2}. \tag{4}$$

The length of sandwich pulses in TIMES is experimentally optimized, but the flip angle of these pulses is always found to be close to the θ value described with Eq. (3). These pulses hence align the z axis of the precession axis, tilted with the phase ramp, with the B_0 field. Under fast MAS, these two axes tend to be very close, and therefore the two sandwich pulses can be dropped, thus leading to the TIMES$_0$ sequence.

It is important to reduce experimentally the number of optimized parameters for quick, stable, and reproducible experimental setup. There are six experimentally adjustable parameters in TIMES: the lengths of sandwich pulses, τ_0, of ramp pulses, τ_p, and of window, τ_w, as well as the amplitudes of rf fields during sandwich pulses, ν_{10}, and ramp pulses, ν_{1p}, and the resonance offset frequency $\Delta\nu_0$. On the other hand, only four parameters (τ_p, ν_{1p}, $\Delta\nu_0$, τ_w) have to be optimized for wPMLG$_{pp}^{x\bar{x}}$ and TIMES$_0$ sequences.

As the interaction and rotating frames coincide every τ_c, the isotropic chemical shift scaling factor can be analytically calculated with first-order average Hamiltonian:

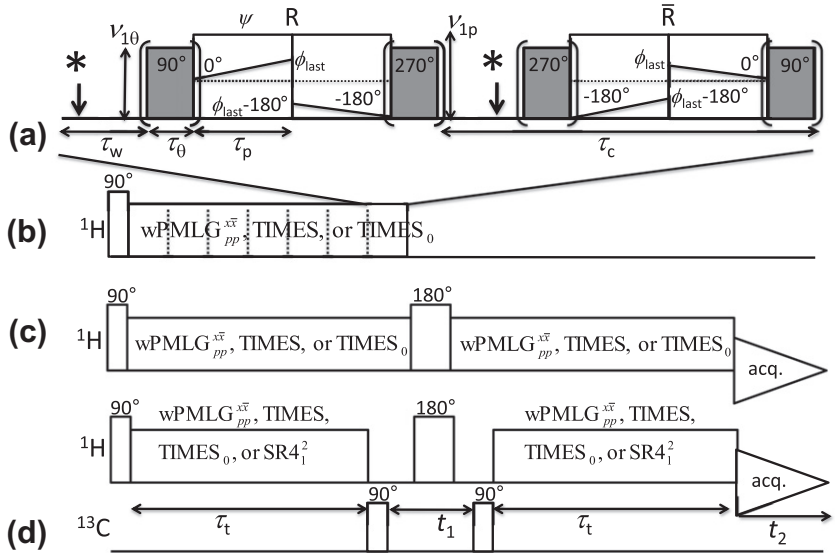

Fig. 1. (a) General pulse scheme for wPMLG$^{x\bar{x}}_{pp}$, TIMES, and TIMES$_0$. NMR signals are sampled during every window at the points indicated by asterisk. z-Rotation is obtained by applying two rotations (R and $\bar{R}$) about two axes symmetrical with respect to B_0. Sandwich gray pulses are omitted in wPMLG$^{x\bar{x}}_{pp}$ and TIMES$_0$. The nutation angles of hard pulses are indicated at the top of each of them and the phases are indicated inside each pulse. The final phase ϕ_{last} is calculated according to Eq. (4) for TIMES and TIMES$_0$ and is fixed to 208° for wPMLG$^{x\bar{x}}_{pp}$. The rf-field strength for sandwich pulses is $\nu_{1\theta}$ and that for ramp pulses is ν_{1p}. (b) 1D ^{1}H NMR pulse sequence. (c) Hahn echo sequence to measure T_2' under ^{1}H decoupling. (d) ^{1}H–{^{13}C} D-HMQC and J-HMQC pulse sequences.

Table 1
Differences in between wPMLG$^{x\bar{x}}_{pp}$, TIMES, and TIMES$_0$.

	wPMLG$^{x\bar{x}}_{pp}$	TIMES	TIMES$_0$
ψ	<360°	360°	360°
ϕ_{last}	208°	Eq. (2)	Eq. (2)
Sandwich pulse	No	Yes	No
Scaling factor	Eq. (5)	Eq. (6)	Eq. (5)

$$\kappa_{cs} = \frac{2\tau_p \cos^2\theta + \tau_w}{\tau_c}, \tag{5}$$

for wPMLG$^{x\bar{x}}_{pp}$ and TIMES$_0$, and

$$\kappa_{cs} = \frac{\frac{2\tau_\theta \sin\theta}{\theta} + 2\tau_p \cos\theta \cos 2\theta + \tau_w}{\tau_c}, \tag{6}$$

for TIMES if the effect of the sandwich pulses are taken into account [41]. The effect of sample spinning is not included in this calculation, since the isotropic chemical shift is not affected by MAS. Thus, we can safely apply these equations even if the cycle time of the sequence is close to that of sample spinning.

3. Experimental

The experiments were performed at 14.1 T with a JEOL JNM-ECA 600 system equipped with a JEOL 1.0 mm double resonance MAS probe. The spinning speed was actively stabilized with a pneumatic solenoid valve so that the spinning fluctuations, averaged over 1 s, are less than 10 Hz. However, a detailed oscilloscope analysis shows that instantaneous fluctuations can increase up to c.a. 30 Hz, especially at ultra-fast speed (e.g. 75–80 kHz). Each phase-ramp pulse was divided into five stripes, with length $\tau_p/5$. Glycine and uniformly ^{13}C, ^{15}N labeled L-alanine samples were purchased from Tokyo Chemical Industry Ltd. and Cambridge Isotope Laboratories, respectively, and used as received without further purification or re-crystallization. All experiments were performed with full rotor samples, without any spacer.

The experimental parameters for direct observation of 1D ^{1}H spectra (Figs. 2 and 3) were optimized so as to achieve the best separation of the two methylene signals of glycine. The rf-strengths were fixed to $\nu_{1\theta} = \nu_{1p} = 125$ kHz, which normally give the best resolution for our spectrometer. The optimization was started on-resonance ($\Delta\nu_0 = 0$), with $\tau_w = 4.8$ μs, and either $\tau_\theta = 0$ for wPMLG$^{x\bar{x}}_{pp}$ and TIMES$_0$, or $\tau_\theta = \theta/2\pi\nu_{1\theta}$ for TIMES. First, τ_p was varied with 100 ns step which corresponds to 20 ns change for each stripe. Then, τ_θ (for TIMES), τ_w, and $\Delta\nu_0$ were finely optimized. The final value of the phase ramp (ϕ_{last}) was not optimized and was either fixed to 208° for wPMLG$^{x\bar{x}}_{pp}$ or directly calculated with Eq. (4) for TIMES and TIMES$_0$.

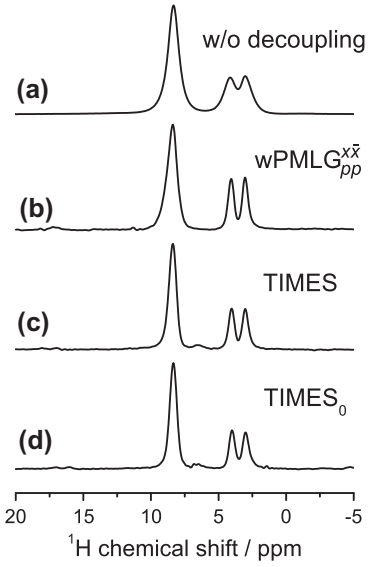

Fig. 2. ^{1}H spectra of glycine without (a) and with (b–d) ^{1}H decoupling at $\nu_r = 80$ kHz MAS. (b–d) Scaled up spectra recorded with (b) wPMLG$^{x\bar{x}}_{pp}$, (c) TIMES, and (d) TIMES$_0$. The frequency scale was divided by the experimentally determined scaling factor to restore the actual chemical shift values. The optimized parameters are (τ_p, τ_w, τ_θ, τ_c, ϕ_{last}, θ, ψ) = (2.80, 4.84, 0, 10.44 μs, and 208°, 31°, 243°) for wPMLG$^{x\bar{x}}_{pp}$, (3.10, 4.82, 0.22, 11.46 μs, and 332°, 23°, 360°) for TIMES, and (3.40, 4.72, 0, 11.52 μs, and 326°, 25°, 360°) for TIMES$_0$.

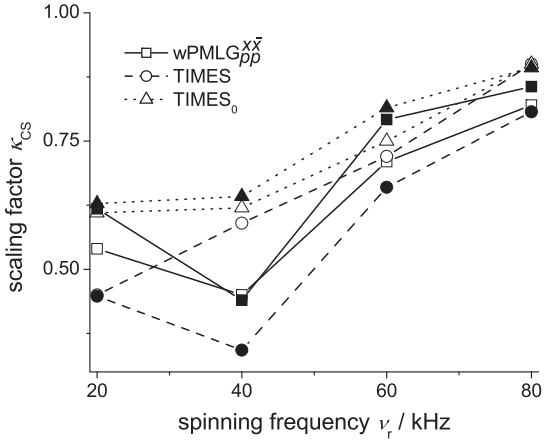

Fig. 3. Experimentally measured (open symbols: Δ, ○, □) and theoretically calculated (filled symbols: ▲, ●, ■) κ_{cs} scaling factors for wPMLG$^{x\bar{x}}_{pp}$ (□, ■), TIMES (○, ●), and TIMES$_0$ (Δ, ▲) homonuclear decoupling at various spinning frequencies.

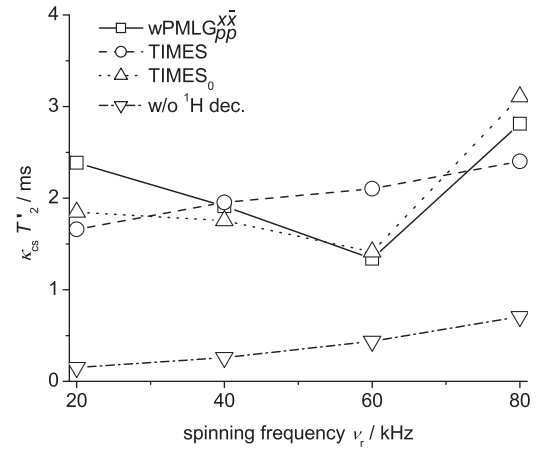

Fig. 4. ^{1}H $\kappa_{cs}T_2'$ averaged value for the two CH_2 protons of glycine at various spinning frequencies. $\kappa_{cs}T_2'$ values are obtained without (▽; κ_{cs} = 1, T_2'), or with wPMLG$^{x\bar{x}}_{pp}$ (□), TIMES (○), and TIMES$_0$ (Δ) ^{1}H–^{1}H decoupling.

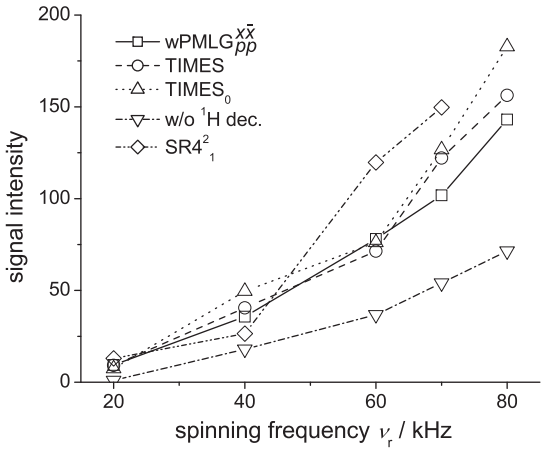

Fig. 5. ^{1}H–{^{13}C} *J*-HMQC-filtered CH signal intensity in uniformly ^{13}C, ^{15}N labeled L-alanine without (▽; κ_{cs} = 1), or with wPMLG$^{x\bar{x}}_{pp}$ (□), TIMES (○), and TIMES$_0$ (Δ) ^{1}H–^{1}H decoupling at various spinning frequencies. The ^{1}H–{^{13}C} *D*-HMQC results obtained with SR4$^2_1$ recoupling are also shown (◇). To achieve a passive rotor-synchronization, we have added a one-rotor delay between SR4$^2_1$ blocks and ^{13}C 90° pulses. The experimental conditions were always optimized to maximize the CH signal intensity. The signal intensities are normalized with respect to that without homonuclear decoupling at MAS of 20 kHz.

For the 1D and 2D *J*-HMQC spectra (Figs. 5 and 6), the optimization for the ^{1}H–^{1}H decoupling started from the values used in Fig. 3 as initial conditions. The parameters were then further optimized with the same order as for 1D experiments, but to maximize the CH peak intensity in *J*-HMQC filtered ^{1}H spectra. Here, a ^{1}H-{^{13}C} *J*-HMQC filtered 1D experiment denotes a ^{1}H-{^{13}C} *J*-HMQC experiment with a null indirect evolution period, t_1 = 0. Finally, the magnetization transfer period, τ_t, was also experimentally optimized for each sequence.

4. Results and discussion

In this section, we evaluate wPMLG$^{x\bar{x}}_{pp}$, TIMES, and TIMES$_0$ in view of points (i–vii) described in Section 1 (summarized in Table 2). It must be first noted that these sequences are designed to have an acquisition window (v) and an effective *z*-rotation (vii).

4.1. 1D spectra

We first observe 1D ^{1}H NMR spectra of glycine, recorded with the sequence shown in Fig. 1b at the speed of ν_r = 80 kHz, to evaluate points (i and ii), the ^{1}H–^{1}H decoupling efficiency and T_2' value at ultra-fast MAS and (iii) the scaling factor. Spectra are shown in Fig. 2, with (b–d) and without (a) ^{1}H–^{1}H decoupling. The ^{1}H rf-field strength of $\nu_{1p} = \nu_{1\theta}$ = 125 kHz was applied to satisfy point (vi), that is, a moderate rf power requirement. For all the decoupling sequences, a much stronger rf-field of $\nu_{1p} \approx 238$ kHz always results in inferior resolution (not shown) [55]. This experimental result demonstrates that large rf-field is not mandatory to achieve efficient homonuclear decoupling under ultra-fast MAS. Note that ^{1}H decoupling gives a much better resolution than ultra-fast MAS alone, even at ν_r = 80 kHz, especially for the two methylene resonances. At that MAS frequency, the three sequences work well with similar ^{1}H resolution as shown in Fig. 2b–d, which shows that requirement (i) is satisfied.

At ultra-fast MAS, a short cycle time is the key point to achieve ^{1}H high resolution, and the cycle time must be shorter than one rotor period [39]; whereas this condition does not lead to good resolution at moderate MAS frequencies [55,56]. In Fig. 2b–d, the cycle times for wPMLG$^{x\bar{x}}_{pp}$, TIMES, and TIMES$_0$ spectra show similar values of τ_c = 10.44, 11.46 and 11.52 μs, respectively, and are all shorter than one MAS rotor period of τ_r = 12.5 μs. All the other experimentally optimized parameters are given in the figure caption. TIMES and TIMES$_0$ decoupling benefit from larger scaling factor κ_{cs} than wPMLG$^{x\bar{x}}_{pp}$ at ν_r = 80 kHz (see Fig. 3). The larger scaling factors result from smaller θ angles (see Eqs. (4) and (5)). Assuming ϕ_{last} = 208° with the experimentally optimized parameters, the calculated rotation angle about the effective field (Eq. (2)) would result in very similar values of ψ = 243°, 250°, and 258° for wPMLG$^{x\bar{x}}_{pp}$, TIMES, and TIMES$_0$. However, TIMES and TIMES$_0$ impose a ψ = 360° rotation, which is obtained by increasing the effective field ν_{eff}, due to further off resonance irradiation ν_{off} than wPMLG$^{x\bar{x}}_{pp}$; this is done by imposing ϕ_{last} values calculated according to Eq. (4). Even with keeping the same ν_{1p} value, the large ν_{off} values in TIMES and TIMES$_0$ result in smaller θ angle (Eq. (3)) than that in wPMLG$^{x\bar{x}}_{pp}$, leading to enhanced scaling factor (Eqs. (5), (6)). It should be noted that short τ_c values also enhance the sensitivity by increasing the duty cycle of acquisition windows. The experimental scaling factors are represented with open symbols versus spinning frequency in Fig. 3. For each MAS frequency, the parameters have been optimized to achieve the best resolution before measuring the scaling factors. These are obtained from the difference between the NH_3^+ signal and the middle of the two CH_2 resonances. At ultra-fast MAS, ν_r = 80 kHz, the requirement of large scaling factor (iii) is satisfied for the three sequences, especially TIMES and TIMES$_0$ which give the largest scaling

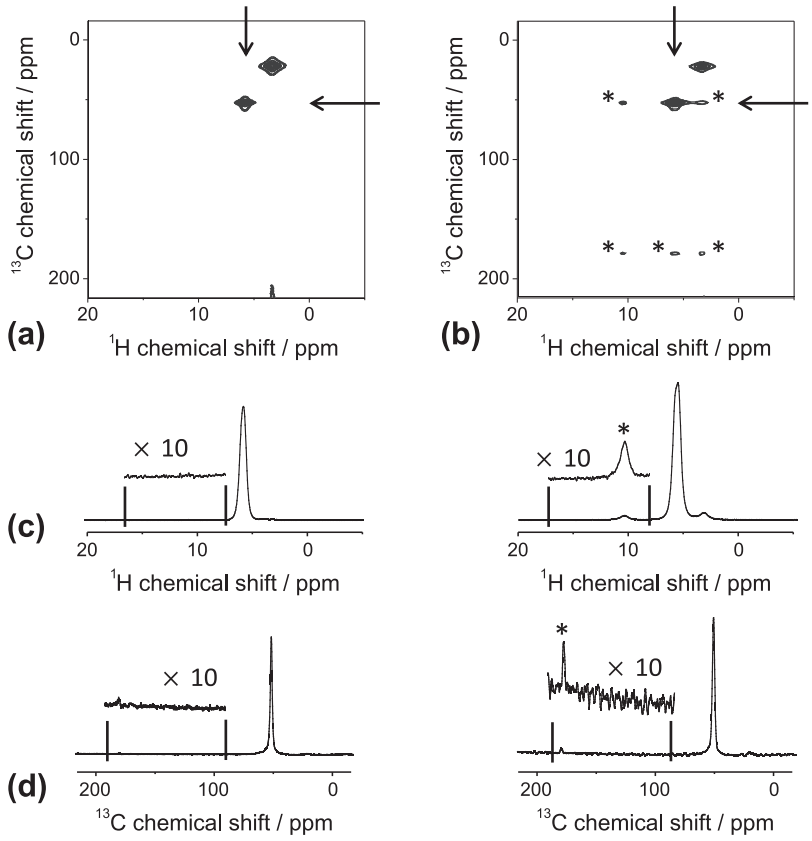

Fig. 6. ^{1}H–{^{13}C} (a) *J*-HMQC and (b) *D*-HMQC spectra at ν_r = 70 kHz of uniformly ^{13}C, ^{15}N labeled L-alanine. TIMES$_0$ with τ_t = 2.02 ms and SR4$_1^2$ with τ_t = 57 μs were applied on the ^{1}H channel during the magnetization transfer periods of *J*-HMQC and *D*-HMQC experiments, respectively. The 2D spectra are plotted with the same contour levels. The (c) ^{1}H and (d) ^{13}C slices of the CH signal, which is indicated by the arrows in (a) and (b), are also shown at the same scale. The insets are magnifications of the slices with a factor of 10. The through-space correlations are indicated by asterisk in *D*-HMQC spectra.

Table 2
Requirements of ^{1}H–^{1}H decoupling schemes for ^{1}H indirect detection.

	wPMLG$_{pp}^{x\bar{x}}$	TIMES	TIMES$_0$
(i) Works at 80 kHz MAS?	Yes	Yes	Yes
(ii) T_2' (ms)	3.43	2.67	3.45
($\kappa_{cs}T_2'$) (ms)	2.81	2.40	3.11
(iii) Scaling factor κ_{cs}	0.82	0.90	0.90
(iv) Number of parameters	4	6	4
(v) Acquisition window	Yes	Yes	Yes
(vi) rf power ν_{1p} (kHz)	125	125	125
(vii) *z*-rotation	Yes	Yes	Yes

factor of κ_{cs} = 0.90, while wPMLG$_{pp}^{x\bar{x}}$ gives a slightly smaller value of κ_{cs} = 0.82. This scaling factor can also be calculated with Eqs. (5), (6) and experimentally optimized τ_p, θ, τ_w, and τ_c values. The results are plotted as filled symbols in Fig. 3, and they agree well with experimental results.

The proton T_2' value, which is observed by Hahn echo MAS experiments, increases linearly with the spinning frequency (Fig. 4). Further enhancement of T_2' value is achieved by applying ^{1}H decoupling during the echo. The corresponding pulse sequence is depicted in Fig. 1c. Here, we compare their *effective* values $\kappa_{cs}T_2'$ for various decoupling schemes. Since ^{1}H chemical shifts and J_{13C-1H} scalar couplings are both scaled by the factor κ_{cs}, $\kappa_{cs}T_2'$ represents the actual effect of signal decay in re-scaled spectra. All three sequences well decouple ^{1}H-^{1}H interactions, leading to much longer $\kappa_{cs}T_2'$ values than the T_2' without decoupling, as shown in Fig. 4. Especially, TIMES$_0$ gives the longest $\kappa_{cs}T_2'$ at 80 kHz MAS, hence satisfying the requirement (ii). In spite of large scaling factor, TIMES shows the shortest $\kappa_{cs}T_2'$ value. This may be due to the effect of sandwich pulses [55]. This unfavorable effect is removed in TIMES$_0$ sequence.

The experimental characters of the wPMLG$_{pp}^{x\bar{x}}$, TIMES, and TIMES$_0$ sequences are listed in (Table 2) in terms of the requirements (i)–(vii). For ease of optimization, wPMLG$_{pp}^{x\bar{x}}$ and TIMES$_0$ are better than TIMES because the formers have two less parameters than the latter. The longest $\kappa_{cs}T_2'$ value is realized by TIMES$_0$, leading to maximum sensitivity in ^{1}H detected experiments (Table 2).

4.2. HMQC spectra

The sensitivity enhancement in HMQC experiments involving coherence transfer via *J* coupling (Fig. 1d) is experimentally demonstrated by Fig. 5, which displays the ^{1}H–{^{13}C} *J*-HMQC filtered ^{1}H signal intensity of the CH peak in uniformly ^{13}C, ^{15}N labeled L-alanine versus spinning frequency. At 80 kHz speed, ^{1}H-^{1}H decoupling irradiation leads to a 2–2.5 sensitivity enhancement with respect to the signal observed without ^{1}H decoupling. The maximum enhancement is achieved by TIMES$_0$ because of its longest $\kappa_{cs}T_2'$ value as predicted from the above discussion. Although the re-scaled linewidths are similar to each other (Fig. 2), the large scaling factors of TIMES and TIMES$_0$ give a significant enhancement in the *J*-HMQC filtered ^{1}H NMR signal intensity.

Similar sensitivity enhancement can be realized by applying a ^{13}C–^{1}H dipolar recoupling sequence. The re-introduction of large D_{13C-1H} dipolar interactions may lead to much faster magnetization transfer between ^{13}C and ^{1}H than with small J_{13C-1H} scalar couplings. We have also tested this experiment, which is called *D*-HMQC, by applying the SR4$_1^2$ recoupling scheme on the proton channel [57,58]. This sequence also presents the advantage of suppressing

the contribution of ^{1}H–^{1}H dipolar interactions to the first-order average Hamiltonian. The ^{1}H–{^{13}C} *D*-HMQC and *J*-HMQC experiments are then very similar and they only differ by the sequence which is applied in the ^{1}H channel (Fig. 1d). Since the recoupled ^{13}C–^{1}H dipolar dephasing depends on the initial rotor-phase, the two $SR4^2_1$ dipolar recoupling periods in the *D*-HMQC sequence must be perfectly rotor-synchronized. The *D*-HMQC data obtained at $\nu_r = 80$ kHz are not shown because the signal intensity was not reproducible due to too large spinning speed fluctuations. Indeed, even a small fluctuation of the instantaneous spinning frequency induces imperfect echo formations [13,59,60]. At $\nu_r = 70$ kHz the fluctuations are much smaller, and the *D*-HMQC sequence then provides the largest signal intensity among the HMQC filtered ($t_1 = 0$) ^{1}H spectra (Fig. 5). Nevertheless, the *J*-HMQC experiment with $TIMES_0$ decoupling results in further signal enhancement at $\nu_r = 80$ kHz, because coherence transfers via scalar couplings are not affected by MAS frequency fluctuations.

We have recorded the ^{1}H–{^{13}C} *D*-HMQC and *J*-HMQC 2D spectra with $SR4^2_1$ recoupling and $TIMES_0$ decoupling, respectively, at $\nu_r = 70$ kHz where the spinning frequency was stable enough to observe *D*-HMQC signal. The two spectra are plotted in Fig. 6 with the same contour levels. ^{13}C and ^{1}H slices of the CH peak are also shown with the same vertical scale. As already observed in Fig. 5, the comparison of the slices in Fig. 6c and d shows a slight enhancement in the intensity of CH peak in favor of *D*-HMQC method using $SR4^2_1$ recoupling compared to *J*-HMQC sequence incorporating $TIMES_0$ homonuclear decoupling. However, it is also clear from Fig. 6d that *D*-HMQC slices exhibit a much stronger t_1-noise along the ^{13}C dimension (indirect dimension) than *J*-HMQC owing to MAS frequency fluctuations. Indeed, it can be noted that the noise intensity in the ^{13}C slices of *D*-HMQC spectrum (see Fig. 6d right) is significantly stronger than in the ^{1}H slice (see Fig. 6c right), whereas no significant difference in noise level is observed between the two spectral dimensions of *J*-HMQC spectrum using $TIMES_0$ decoupling (compare Fig. 6c,d left). This strong t_1-noise, due to $SR4^2_1$, negates the slight signal enhancement observed in *D*-HMQC. *J*-HMQC spectra are more useful than *D*-HMQC spectra for spectral assignments, since they only display through-bond correlations, whereas *D*-HMQC spectra show through-space correlations. We can clearly see several through-space correlations (indicated by $*$) in *D*-HMQC spectra (Fig. 6b), which do not appear with *J*-HMQC sequence (Fig. 6a).

The build-up curves observed at $\nu_r = 70$ kHz, versus the length τ_t of each recoupling period are shown in Fig. 7. They are dominated by two competing effects: the T_2' or $\kappa_{cs}T_2'$ relaxation coefficient and the magnetization transfer rate. The transfer rate is solely determined by the size of the recoupled interaction between ^{13}C and ^{1}H for both CH and CH_3 groups, in which the spins behave just as a summation of CH systems in the case of ^{1}H observation [61]. In *D*-HMQC, the maximum signal intensity of CH is observed at around $\tau_t \approx 57$ μs (Fig. 7c), which is close to the theoretical value of $\tau_t \approx 70$ μs [62]. The optimal condition for CH_3 is very different from that for CH and close to $\tau_t \approx 143$ μs (Fig. 7d). This is because of the smaller dipolar interaction in CH_3, which is one-third that in CH owing to the fast rotation of the methyl group. On the other hand, *J*-couplings, which drive the magnetization transfer in *J*-HMQC experiments, have similar values of $J_{13C-1H} \approx 140$ Hz both for CH and CH_3 groups since they are not affected by the rotation of the methyl group. This results in the fact that the maximum signal intensity is obtained at the same τ_t value both for CH and for CH_3 groups (Fig. 7a and b). The optimal condition of $\tau_t \approx 2.0$ ms is smaller than the theoretical value of $\tau_t \approx 0.5/\kappa_{cs}J_{13C-1H}) \approx 4.2$ ms. This decrease shows that the $\kappa_{cs}T_2'$ value of 2–3 ms (Fig. 4) still has significant effect on build up curve in *J*-HMQC experiments. The difference between *D*-HMQC and *J*-HMQC build-up curves can also be observed in Fig. 6. Indeed, since the τ_t values have been optimized to maximize the CH intensity, much weaker CH_3 signal appear in *D*-HMQC (Fig. 6b) than in *J*-HMQC (Fig. 6a). *J*-HMQC should thus be preferred to *D*-HMQC to obtain a more uniform excitation.

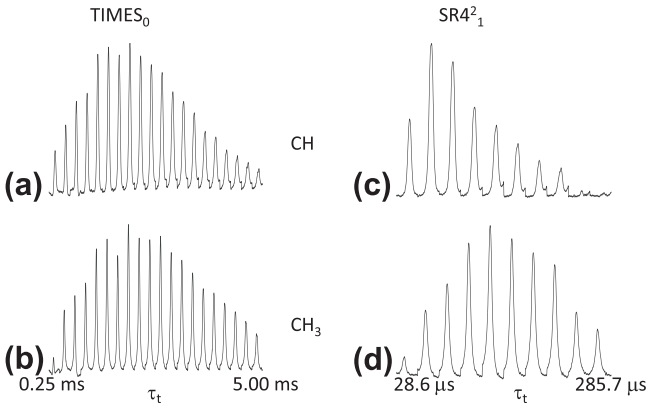

Fig. 7. ^{1}H–{^{13}C} HMQC-filtered ^{1}H NMR signal intensity of uniformly ^{13}C, ^{15}N labeled L-alanine as function of τ_t time at $\nu_r = 70$ kHz. $TIMES_0$ decoupling (*J*-HMQC; a and b) and $SR4^2_1$ recoupling (*D*-HMQC; c and d) were applied during magnetization transfer periods. The signal intensities of CH (a and c) and CH_3 (b and d) are shown.

5. Conclusions

We have demonstrated three ^{1}H–^{1}H homonuclear dipolar decoupling sequences for enhancing the magnetization transfer efficiency between ^{13}C and ^{1}H in the ^{1}H–{^{13}C} *J*-HMQC experiments. Indeed, in addition to $wPMLG^{x\bar{x}}_{pp}$ and TIMES sequences, we have proposed another TIMES version without the bracketing pulses, named $TIMES_0$. This simplification can be safely applied only at very fast MAS regime where the bracketing pulses become negligible with small θ. In the TIMES and $TIMES_0$ sequences, the angle θ between the magnetic field and the effective field is adjusted, while keeping the rotation angle about the effective field fixed to $\psi = 360°$. When the effective field tends to align with the B_0 field, the chemical shift scaling factor κ_{cs} increases at the expense of a wider line-width since the suppression of ^{1}H–^{1}H dipolar interaction becomes less efficient. The best compromise in terms of resolution is thus obtained experimentally by optimizing the θ value. Since the phase ramp is systematically calculated from equations, $TIMES_0$ does not introduce any additional adjustable parameter compared to $wPMLG^{x\bar{x}}_{pp}$. At ultra-fast MAS ($\nu_r = 80$ kHz), which is presently the fastest commercially available speed, and with the moderate rf-field strength of c.a. 120–130 kHz, TIMES and $TIMES_0$ benefit from the very large chemical-shift scaling factors of $\kappa_{cs} = 0.90$, as well as from a high resolution comparable to that observed with $wPMLG^{x\bar{x}}_{pp}$. $TIMES_0$, which has the advantage of only four adjustable parameters for easy setup, is suitable for ^{1}H–{^{13}C} through-bond *J*-HMQC measurements at ultra-fast MAS in terms of large scaling factor, and efficient homonuclear decoupling. Although similar sensitivity enhancement can be obtained with through-space *D*-HMQC experiments, *J*-HMQC spectra incorporating ^{1}H-^{1}H decoupling have the advantages of lower t_1-noise and more uniform excitation of both CH, CH_2 and CH_3 groups. Furthermore, *J*-HMQC provides unambiguous ^{13}C–^{1}H through-bond correlations, which help spectral assignment.

Acknowledgments

Authors are grateful for funding provided by Region Nord/Pas de Calais, Europe (FEDER), CNRS, French Minister of Science, USTL, ENSCL, and CortecNet. Financial support from the TGIR RMN THC (FR-3050) for conducting the research is gratefully acknowledged.

References

[1] A.A. Maudsley, L. Müller, R.R. Ernst, Cross-correlation of spin-decoupled NMR spectra by heteronuclear two-dimensional spectroscopy, J. Magn. Reson 28 (1977) 463–469.

[2] L. Müller, Sensitivity enhanced detection of weak nuclei using heteronuclear multiple quantum coherence, J. Am. Chem. Soc. 101 (1979) 4481–4484.

[3] A. Bax, R.H. Griffey, B.L. Hawkins, Correlation of proton and nitrogen-15 chemical shifts by multiple quantum NMR, J. Magn. Reson. 55 (1983) 301–315.

[4] J.W. Wiench, C.E. Bronnimann, S.Y. Victor, M. Pruski, Chemical-shift correlation NMR spectroscopy with indirect detection in fast rotating solids: studies of organically functionalized mesoporous silicas, J. Am. Chem. Soc. 129 (2007) 12076.

[5] Y. Ishii, R. Tycko, Sensitivity enhancement in solid state ^{15}N NMR by indirect detection with high-speed magic angle spinning, J. Magn. Reson. 142 (2000) 199–204.

[6] D.H. Zhou, J.J. Shea, A.J. Nieuwkoop, W.T. Franks, B.J. Wylie, C. Mullen, D. Sandoz, C.M. Rienstra, Solid-state protein-structure determination with proton-detected triple-resonance 3D magic-angle-spinning NMR spectroscopy, Angew. Chem. Int. Ed. 46 (2007) 8380.

[7] Donghua, H. Zhou, G. Shah, M. Cormos, C. Mullen, D. Sandoz, C.M. Rienstra, Proton-detected solid-state NMR spectroscopy of fully protonated proteins at 40 kHz magic-angle spinning, J. Am. Chem. Soc. 129 (2007) 11791–11801.

[8] I. Schnell, B. Langer, S.H.M. Sontjens, M.H.P. van Genderen, R.P. Sijbesma, H.W. Spiess, Inverse detection and hetero-nuclear editing in ^{1}H–^{15}N correlation and ^{1}H–^{1}H double-quantum NMR spectroscopy in the solid state under fast MAS, J. Magn. Reson. 150 (2001) 57–70.

[9] I. Schnell, K. Saalwachter, ^{15}N–^{1}H bond length determination in natural abundance by inverse detection in fast-MAS solid-state NMR spectroscopy, J. Am. Chem. Soc. 124 (2002) 10938–10939.

[10] Y. Ishii, J.P. Yesinowski, R. Tycko, Sensitivity enhancement in solid-state ^{13}C NMR of synthetic polymers and biopolymers by ^{1}H NMR detection with high-speed magic angle spinning, J. Am. Chem. Soc. 123 (2001) 2921–2922.

[11] H. Donghua, D. Zhou, C.M. Rienstra, Rapid analysis of organic compounds by proton-detected hetero-nuclear correlation NMR spectroscopy with 40 kHz magic-angle spinning, Angew. Chem. Int. Ed. 47 (2008) 7328–7331.

[12] A. Samoson, T. Tuherm, J. Past, A. Reinhold, T. Anupold, I. Heinmaa, New horizons for magic-angle spinning NMR, Top. Curr. Chem. 246 (2004) 15–31.

[13] Y. Nishiyama, Y. Endo, T. Nemoto, H. Utsumi, K. Yamauchi, K. Hioka, T. Asakura, Very fast magic angle spinning ^{1}H–^{14}N 2D solid-state NMR: sub-micro-liter sample data collection in a few minutes, J. Magn. Reson. 208 (2011) 44–48.

[14] P. Hodgkinson, High-resolution ^{1}H NMR spectroscopy of solids, Annu. Rep. NMR Spec. 72 (2011) 185–223.

[15] W.I. Goldburg, M. Lee, Nuclear magnetic resonance line narrowing by a rotating rf field, Phys. Rev. Lett. 11 (1963) 255–258.

[16] M. Lee, W.I. Goldburg, Nuclear-magnetic-resonance line narrowing by a rotating rf field, Phys. Rev. 140 (1965) 1261.

[17] J.S. Waugh, L.M. Huber, Method for observing chemical shifts in solids, J. Chem. Phys. 47 (1967) 1862–1863.

[18] J.S. Waugh, L.M. Huber, U. Haeberlen, Approach to high-resolution NMR in solids, Phys. Rev. Lett. 20 (1968) 180–182.

[19] K. Takegoshi, C.A. McDowell, A "Magic Echo" pulse sequence for the high-resolution NMR spectra of abundant spins in solids, Chem. Phys. Lett. 116 (1985) 100.

[20] A. Bielecki, A.C. Kolbert, M.H. Levitt, Frequency-switched pulse sequences: homonuclear decoupling and dilute spin NMR in solids, Chem. Phys. Lett. 155 (1989) 341–346.

[21] B.M. Fung, K. Ermolaev, Y. Yu, ^{13}C NMR of liquid crystals with different proton homonuclear dipolar decoupling methods, J. Magn. Reson. 138 (1999) 28–35.

[22] E. Vinogradov, P.K. Madhu, S. Vega, High-resolution proton solid-state NMR spectroscopy by phase modulated Lee–Goldburg experiment, Chem. Phys. Lett. 314 (1999) 443–450.

[23] B.C. Gerstein, R.G. Pembleton, R.C. Wilson, L.M. Ryan, High resolution NMR in randomly oriented solids with homonuclear dipolar broadening: combined multiple pulse NMR and magic angle spinning, J. Chem. Phys. 66 (1977) 361–362.

[24] B.C. Gerstein, in: D.M. Grant, R.K. Harris (Eds.), Encyclopedia of Nuclear magnetic Resonance, Wiley, New York, 2002.

[25] D.E. Demco, S. Hafner, H.W. Spiess, Rotation-synchronized homonuclear dipolar decoupling, J. Magn. Reson. A 116 (1995) 36–45.

[26] P.K. Madhu, X. Zhao, M.H. Levitt, High-resolution ^{1}H NMR in the solid state using symmetry-based pulse sequences, Chem. Phys. Lett. 346 (2001) 142–148.

[27] S. Paul, R.S. Thakur, P.K. Madhu, ^{1}H homonuclear decoupling at high magic-angle spinning frequencies with rotor-synchronized symmetry sequences, Chem. Phys. Lett. 456 (2008) 253–256.

[28] S. Paul, R.S. Thakur, M.H. Levitt, P.K. Madhu, ^{1}H homonuclear dipolar decoupling using rotor-synchronized pulse sequences: towards pure absorption phase spectra, J. Magn. Reson. 205 (2010) 269–275.

[29] J.-P. Amoureux, B. Hu, J. Trébosc, Enhanced resolution in proton solid-state NMR with very-fast MAS experiments, J. Magn. Reson. 193 (2008) 305–307.

[30] J.-P. Amoureux, B. Hu, J. Trébosc, Q. Wang, O. Lafon, F. Deng, Homonuclear dipolar decoupling schemes for fast MAS, Solid State Nucl. Magn. Reson. 35 (2009) 19–24.

[31] O. Lafon, Q. Wang, B. Hu, J. Trébosc, J.P. Amoureux, F. Deng, Proton–proton homonuclear dipolar decoupling in solid state NMR using rotor-synchronized z-rotation pulse sequences, J. Chem. Phys. 130 (2009) 014504.

[32] S. Paul, D. Schnider, P.K. Madhu, ^{1}H homonuclear dipolar decoupling using symmetry-based pulse sequences at ultra fast magic-angle spinning frequencies, J. Magn. Reson. 206 (2010) 241–245.

[33] M. Leskes, S. Steuernagel, D. Schneider, P.K. Madhu, S. Vega, Homonuclear dipolar decoupling at magic-angle spinning frequencies up to 65 kHz in solid-state nuclear magnetic resonance, Chem. Phys. Lett. 466 (2008) 95–99.

[34] L. Mafra, R. Siegel, C. Fernandez, D. Schneider, F. Aussenac, J. Rocha, High-resolution ^{1}H homonuclear dipolar recoupling NMR spectra of biological solids at MAS rates up to 67 kHz, J. Magn. Reson. 199 (2009) 111–114.

[35] D. Sakellariou, A. Lesage, P. Hodgkinson, L. Emsley, Homonuclear dipolar decoupling in solid-state NMR using continuous phase modulation, Chem. Phys. Lett. 319 (2000) 253–260.

[36] A. Lesage, D. Sakellariou, S. Hediger, B. Elena, P. Charmont, S. Steuernagel, L. Emsley, Experimental aspects of proton NMR spectroscopy in solids using phase-modulated homonuclear dipolar decoupling, J. Magn. Reson. 162 (2003) 105–113.

[37] B. Elena, G. de Paeepe, L. Emsley, Direct spectral optimization of proton–proton homonuclear dipolar decoupling in solid-state NMR, Chem. Phys. Lett. 398 (2004) 532–538.

[38] E. Salager, R.S. Stein, S. Steuernagel, A. Lesage, B. Elena, L. Emsley, Enhanced sensitivity in high-resolution ^{1}H solid-state NMR spectroscopy with DUMBO dipolar decoupling under ultra-fast MAS, Chem. Phys. Lett. 469 (2009) 336–341.

[39] M. Leskes, P.K. Madhu, S. Vega, Why does PMLG proton decoupling work at 65 kHz MAS?, J Magn. Reson. 199 (2009) 208–213.

[40] E. Salager, J.-N. Dumez, R.S. Stein, S. Steuernagel, A. Lesage, B. Elena-Herrmann, L. Emsley, Homonuclear dipolar decoupling with very large scaling factors for high-resolution ultra-fast magic angle spinning ^{1}H solid-state NMR spectroscopy, Chem. Phys. Lett. 498 (2010) 214–220.

[41] Z. Gan, P.K. Madhu, J.-P. Amoureux, J. Trebosc, O. Lafon, A tunable homonuclear dipolar decoupling scheme for high-resolution proton NMR of solids from slow to fast magic-angle spinning, Chem. Phys. Lett. 503 (2011) 167–170.

[42] M. Mehring, J.S. Waugh, Magic-angle NMR experiments in solids, Phys. Rev. B 5 (1972) 3459–3471.

[43] M.H. Levitt, A.C. Kolbert, A. Bielecki, D.J. Ruben, High-resolution ^{1}H NMR in solids with frequency-switched multiple-pulse sequences, Solid State Nucl. Magn. Reson. 2 (1993) 151–163.

[44] K. Yamauchi, S. Kuroki, I. Ando, The amide proton NMR chemical shift and hydrogen-bonded structure of glycine-containing peptides and polypeptides in the solid state as studies by multi-pulse-associated high-speed MAS ^{1}H NMR, J. Mol. Struct. 602–603 (2002) 9–16.

[45] E. Vinogradov, P.K. Madhu, S. Vega, Proton spectroscopy in solid state nuclear magnetic resonance with windowed phase modulated Lee–Goldburg decoupling sequences, Chem. Phys. Lett. 354 (2002) 193–202.

[46] M. Leskes, P.K. Madhu, S. Vega, A broad-banded z-rotation windowed phase-modulated Lee–Goldburg pulse sequence for ^{1}H spectroscopy in solid-state NMR, Chem. Phys. Lett. 447 (2007) 370–374.

[47] M. Leskes, P.K. Madhu, S. Vega, Super-cycled homonuclear dipolar decoupling in solid-state NMR: toward cleaner ^{1}H spectrum and higher spinning rates, J. Chem. Phys. 128 (2008) 052309.

[48] S. Paul, R.S. Thakur, M. Goswami, A.C. Sauerwein, S. Mamone, M. Concistre, H. Forster, M.H. Levitt, P.K. Madhu, Super-cycled homonuclear dipolar decoupling sequences in solid-state NMR, J. Magn. Reson. 197 (2009) 14–19.

[49] M. Leskes, P.K. Madhu, S. Vega, Proton line narrowing in solid-state nuclear magnetic resonance: new insights from windowed phase-modulated Lee–Goldburg sequence, J. Chem. Phys. 125 (2006) 124506.

[50] K. Mao, J.W. Wiench, V.S.Y. Lin, M. Pruski, Indirectly detected through-bond chemical shift correlation NMR spectroscopy in solids under fast MAS: studies of organic–inorganic hybrid materials, J. Magn. Reson. 196 (2009) 92–95.

[51] K. Mao, M. Pruski, Directly and indirectly detected through-bond hetero-nuclear correlation solid-state NMR spectroscopy under fast MAS, J. Magn. Reson. 201 (2009) 165–174.

[52] G.P. Holland, B.R. Cherry, J.E. Jenkins, J.L. Yarger, Proton-detected hetero-nuclear single quantum correlation NMR spectroscopy in rigid solids with ultra-fast MAS, J. Magn. Reson. 202 (2010) 64–71.

[53] A. Lesage, D. Sakellariou, S. Steuernagel, L. Emsley, Carbon-Proton chemical shift correlation in solid-state NMR by through-bond multiple-quantum spectroscopy, J. Am. Chem. Soc. 120 (1998) 13194–13201.

[54] K. Mao, M. Pruski, Homonuclear dipolar decoupling under fast MAS: resolution patterns and simple optimization strategy, J. Magn. Reson. 203 (2010) 144–149.

[55] V.E. Zorin, M. Ernst, S.P. Brown, P. Hodgkinson, Insights into homonuclear decoupling from efficient numerical simulation: techniques and examples, J. Magn. Reson. 192 (2008) 183–196.

[56] E. Vinogradov, P.K. Madhu, S. Vega, Phase modulated Lee–Goldburg magic angle spinning proton nuclear magnetic resonance experiments in the solid-state: a bimodal Floquet theory treatment, J. Chem. Phys. 115 (2001) 8983–9000.

[57] A. Brinkmann, A.P.M. Kentgens, Proton-selective ^{17}O–^{1}H distance measurements in fast magic-angle-spinning solid-state NMR spectroscopy for the determination of hydrogen bond lengths, J. Am. Chem. Soc. 128 (2006) 14758–14759.
[58] O. Lafon, Q. Wang, B. Hu, F. Vasconcelos, J. Trébosc, S. Cristol, F. Deng, J.-P. Amoureux, Indirect detection via spin-1/2 nuclei in solid state NMR spectroscopy: application to the observation of proximities between protons and quadrupolar nuclei, J. Phys. Chem. A 113 (2009) 12864–12878.
[59] L. Chen, Q. Wang, B. Hu, O. Lafon, J. Trébosc, F. Deng, J.-P. Amoureux, Measurement of hetero-nuclear distances using a symmetry-based pulse sequence in solid-state NMR, Phys. Chem. Chem. Phys. 12 (2010) 9395–9405.
[60] J. Trébosc, O. Lafon, B. Hu, J.-P. Amoureux, Indirect high-resolution detection for quadrupolar spin-3/2 nuclei in dipolar HMQC solid-state NMR experiments, Chem. Phys. Lett. 496 (2010) 201–207.
[61] J.-P. Amoureux, J. Trébosc, J. Wiench, M. Pruski, HMQC and refocused-INEPT experiments involving half-integer quadrupolar nuclei in solids, J. Magn. Reson 184 (2006) 1–14.
[62] Q. Wang, X. Lu, O. Lafon, J. Trébosc, F. Deng, B. Hu, Q. Chen, J.-P. Amoureux, Measurement of ^{13}C–^{1}H dipolar couplings in solids by using ultra-fast magic-angle spinning NMR spectroscopy with symmetry-based sequences, Phys. Chem. Chem. Phys. 13 (2011) 5967–5973.